METEOROID IMPACTS AS SOURCES OF SEISMICITY ON THE MOON

Arthur McGarr and Gary V. Latham
Lamont-Doherty Geological Observatory of Columbia University
Palisades, New York 10964

Donald E. Gault
Ames Research Center, Moffett Field, California 94035

Technical Report No. 1
CU-1-69
National Aeronautics and Space Administration
Contract NAS 9-5957

February 1969

METEOROID IMPACTS AS SOURCES OF SEISMICITY ON THE MOON

Arthur McGarr[1] and Gary V. Latham
Lamont-Doherty Geological Observatory of Columbia University
Palisades, New York 10964

Donald E. Gault
Ames Research Center, Moffett Field, California 94035

Technical Report No. 1
CU-1-69
National Aeronautics and Space Administration
Contract NAS 9-5957

February 1969

[1] Presently at the Bernard Price Institute of Geophysical Research, University of the Witwatersrand, Johannesburg, South Africa

Digitized by the Internet Archive
in 2020 with funding from
Columbia University Libraries

https://archive.org/details/meteoroidimpacts00mcga

CONTENTS

ABSTRACT 1

INTRODUCTION 1

EXPERIMENTAL EVIDENCE 3
- Experimental setup 3
- Experimental results 4

ANALYSIS OF DATA 5
- Unconsolidated sand 7
- Bonded sand 7
- Impacts and explosions 9
- Momentum conservation 9

NUMBER OF DETECTABLE METEOROID IMPACTS 10
- Artificial impact sources 14
- Conclusions 14

ACKNOWLEDGMENTS 14

TABLES 16

REFERENCES 22

FIGURES 24

APPENDIX I 34

APPENDIX II 37

ABSTRACT

In conjunction with the Apollo Lunar Passive Seismic Experiment, a study was undertaken to determine the efficiency of meteoroid impacts on the lunar surface as potential sources of seismic energy. This study is based on experiments performed at Ames Research Center to determine the coupling between an impacting projectile and seismic waves. High-velocity guns at Ames were used to fire projectiles into targets in a vacuum chamber. Projectile velocities ranged from less than 1 km/sec to more than 7 km/sec and projectile masses from about 0.25 gm to 5 gm. Targets were of two types having considerably different elastic properties. Experimental results indicate that the seismic source function of an impact can be expressed as a function of the kinetic energy of the projectile. Extrapolating our results up to the kinetic energies of meteoroids, it is possible to predict the numbers of impacts that will be detected by the Apollo Passive Seismic Experiment during its nominal lifetime of one year if assumptions are made regarding the physical properties of the moon. For the most optimistic set of assumptions, the instrument will detect about 370 meteoroid impacts; and for the most pessimistic, about 3 impacts. Most of these will be within 10 to 20 km from the seismometers.

The experimental data of this study can be used to estimate the effectiveness of impacting spent spacecraft stages as artificial seismic sources. The results suggest that surface waves generated by the impact of the Saturn S-IVB stage of the Apollo booster would be detected at distances of from 41 to 681 kms from the seismometer depending on the properties assumed for the lunar surface material.

INTRODUCTION

Two seismic experiments are planned as part of the Apollo manned lunar landing program: a passive seismic experiment and an active seismic experiment. The primary purpose of the passive seismic experiment is to detect naturally occurring lunar seismic activity; whereas, the active experiment will include a series of explosive sources. The instrumentation for the passive seismic experiment consists of three long-period seismometers (15 sec natural periods) and one short-period, vertical component seismometer (1 sec natural period). The sensors for the active seismic experiment are three geophones with signal bandwidth from 3 Hz to 250 Hz. As planned, data will be telemetered back to earth from the passive experiment sensors for a period of one year with intermittent transmissions from the active experiment sensors.

There are two possible sources of natural seismic activity on the moon: (1) "moon quakes", i.e., seismic energy released by sudden rupture or changes in volume within the moon; and (2) meteoroids colliding with the lunar surface. The objective of the research reported here is to estimate the number and character of seismic signals produced by meteoroid impacts on the moon that will be recorded during the lifetime of the Apollo seismic experiments.

Seismicity due to meteoroid impacts has been the subject of several previous studies; notably those of Press et al. [1960] and Laster and Press [1968]. The basic assumption in each of these studies is that there is an equivalence between seismic signals from underground nuclear explosions of a given yield and from hypothetical impacts of meteoroids having kinetic energy equal to the yield. Press et al. [1960] used meteorite statistics of Brown [1960] plus a number of assumptions regarding meteoroid velocities and lunar structure to conclude that between 2 and 8 events per year would be recorded by a seismometer with a threshold sensitivity of one millimicron if inelastic attenuation were absent, and one event every three to ten years if attenuation were 0.002/km. Laster and Press [1968] used new meteorite statistics proposed by Shoemaker [1966] to update the previous estimate and concluded that between 6400 and 250 surface wave events would be recorded per year assuming lunar structure proposed by Phinney and Anderson [1965] and a quality factor, Q, of 300.

In the present study, no equivalence between underground nuclear explosions and meteoroid impacts is assumed. Rather, the coupling between impacting projectiles and seismic waves was determined from experiments performed in the laboratory. The experiments, performed at the vertical gun facility at Ames Research Center, consisted of impacting projectiles of various masses and velocities into targets, of two different materials, in a vacuum chamber. The resulting seismic waves were recorded by an array of miniature accelerometers implanted on the targets.

Even with the more direct estimate of coupling between impacting meteoroids and seismic waves presented here, there is still considerable uncertainty in a study such as this. Firstly, we can only guess at the physical properties of the moon, and secondly, our knowledge of the meteoroid flux distribution in the vicinity of the earth-moon system is limited. Our experiments indicate that the fraction of the total projectile kinetic energy which is converted into seismic wave energy is strongly dependent upon the type of target material. Therefore, the rationale employed in this study was to select extreme model parameters such that the estimates of detectable meteoroids will represent upper and lower limits on expected values.

A secondary objective of this study is to determine the effectiveness of impacts of missiles or spent spacecraft propulsion-stages as sources of seismic energy. Such sources, with known origin times and locations, will provide important additions to lunar travel-time data, just as nuclear tests have provided data for improved travel times for the earth.

In summary, our approach is to use laboratory experiments to obtain seismic source functions for impacts. The empirical source functions are then combined with the meteoroid flux statistics given by Hawkins [in Cosby and Lyle, 1965] to obtain the distribution of seismic sources on the lunar surface. The last step in the analysis was to use the distance-amplitude relationships for seismic waves given by Haskell [1957], to obtain an estimate for the number of detectable seismic waves from meteoroid impacts over a one-year period.

EXPERIMENTAL EVIDENCE

Experimental setup. A schematic diagram of the vertical gun facility at Ames Research Center is shown in Figure 1. Projectiles were fired from a two-stage light-gas gun into targets in a chamber which had been evacuated to a pressure of about 300 microns. In the gas gun an explosively driven piston is used to compress a light-gas propellant (He or H_2) which, in turn, accelerates the projectile [Kinslow, 1965]. The powder gun is similar to an ordinary rifle. The projectiles were cylindrical in shape and made of plastic (lexan). They ranged in mass from about 0.25 gm to 5 gm and were impacted at normal incidence with velocities ranging from about 0.8 km/sec to more than 7 km/sec. Projectile velocities of less than 4 km/sec were achieved by using a powder gun instead of the gas gun. When required, a plexiglass shield was used to protect the target from the exhaust products of the gun.

As shown in Figure 1, two types of targets were used. One type was a cylindrical Fiberglass bucket, 33 cm deep and 122 cm in diameter, filled with unconsolidated quartz sand. The other type was a metal bucket about 15 cm deep and 57.5 cm in diameter filled with sand grains bonded together with epoxy cement. The bonded sand mixture had considerably higher seismic velocities than the unconsolidated sand. Table 1 lists bulk properties for both target materials.

Seismic waves produced by the impacts were detected with an array of four miniature accelerometers spaced along a diameter of the target as shown in Figure 1. The accelerometers have a flat response to acceleration for frequencies ranging from near DC to more than 8 Khz, which is quite adequate for the present study. The seismic signals were recorded both on a high-speed chart recorder and on magnetic tape.

Experimental Results. Figure 2 shows impact craters and accelerometer arrays for both types of targets. The craters in the two different targets have a considerably different appearance. The craters shown in Figures 2a and 2b are typical of impact craters in fragmental materials having no rigidity and craters in "hard rock", respectively. Ejecta from craters formed in loose sand consistently include some shock-welded agregates of the granular material when the impact velocity is greater than 3 or 4 km/sec. This so-called "instant rock" is, however, an insignificant fraction of the total ejected mass which consists primarily of single grains of sand. In contrast, the mass of the largest fragments of ejecta from hard-rock craters may be hundreds of times greater than the projectile mass; dimensionally, the ejecta fragments may approach an order of magnitude larger.

Figure 3 shows seismic signals as recorded on both types of targets. The signal recorded on the bonded sand is very sinusoidal with a prominent frequency of about 7 Khz. For shots into bonded sand, the predominant signal frequency ranged from about 5 to 7 Khz. The character of the signals recorded in the bonded sand is primarily determined by the frequencies of the normal modes of vibration of the targets rather than by the time history of the source function because the seismic wavelengths are comparable to the target dimensions. In Figure 4, we see that the spectrum of acceleration amplitude consists of a series of well-defined peaks, the most prominent being a peak at about 7 Khz. Most of these peaks can be identified with a resonant mode of vibration of the target.

Signals recorded in unconsolidated sand have an impulsive character (Figure 3) with most of the spectral amplitude in the frequency band of 0.5 to 1.5 Khz (Figure 5). The sand behaves very much like a liquid in that the shear velocity is negligible compared to the compressional velocity, which is itself very low (Table 1). Because of the low seismic velocity, the wavelengths are small (about 13 cm) relative to the target dimensions and so the finite extent of the sand target has little, if any, effect on the recorded signals. Thus, the signals recorded in the sand targets correspond primarily to the time history of the seismic source.

Peak acceleration was measured for each shot directly from the high-speed paper records. For the shots into bonded sand, peak acceleration is taken to be half of the maximum peak-to-peak signal amplitude. For the shots into unconsolidated sand, the amplitude of the first half-cycle was used. The measured values are listed in Table 2 for accelerometers 1 and 2. Accelerometer numbers 1 and 2 are the most distant and second most distant from the impact point. Generally, the accelerations recorded on the bonded

sand targets are 2 to 3 orders of magnitude greater than those recorded in sand. Figure 6 shows averages of the amplitudes of acceleration listed in Table 2 plotted as a function of the kinetic energy of the impacting projectile on a log-log scale for both types of targets. Straight lines were fitted to both sets of data by a least-squares process. The resulting slopes of the lines are 0.65 for the bonded sand and 0.34 for the sand. The straight line in Figure 4a appears to describe the data reasonably well whereas in Figure 4b the slope of the data would have been of the order of 1/2 if shots 40, 52, and 58 had been omitted. These three projectiles were the only ones that impacted at velocities less than sonic velocity (2.12 km/sec for the bonded sand). Thus, the peak acceleration as measured at a fixed distance from the point of impact varies approximately as $E^{1/3}$ for sand and $E^{1/2}$ to $E^{2/3}$ for bonded sand, where E is the kinetic energy of the projectile.

ANALYSIS OF DATA

Energy Scaling. In many respects, impacts appear to be similar to shallow explosions [Kinslow, 1965; Short, 1966]. This suggests the possibility of applying scaling laws similar to those used to describe explosion phenomena [Cole, 1948; Chabai, 1965] to the problem of the production of seismic waves by impact. According to Chabai [1965] quantities that have dimensions of length or time scale as $E^{1/3}$, where E is the energy released by the explosion or, in our case, the projectile kinetic energy.

Source Functions. A thorough discussion of the physical phenomena that occur when a projectile impacts a target at hypervelocity was presented by Gault et al. [1968]. In this study we are concerned only with the processes that occur outside the zone of inelastic wave propagation and not with the phenomena that occur in the region where material is stressed beyond its elastic limits.

For purposes of analysis, we assume a simple model for the seismic source function, namely, a time-dependent stress acting downward on the free surface of the target. In a circular-cylindrical coordinate system, with the impact point at the origin, the boundary conditions on the upper free-surface of the target are

$$P_{zr}(r,o,t) = 0$$

$$P_{zr}(r,o,t) = S(1 - \cos w_1 t) \qquad (1)$$

$$\text{for} \quad r \leq a, \qquad o \leq t \leq \frac{2}{w_1}$$

$$P_{zz}(r,o,t) = 0 \quad \text{for} \quad r > a, \quad o > t > \frac{2}{w_1}$$

where P_{zr} and P_{zz} are tangential and normal stresses. S is the amplitude of the applied stress, W_1 is the angular frequency of the source function, and $\underline{a}$ is the radius of the source area. The time dependence of the source was suggested by the signals recorded in sand (Figure 3) which are similar in appearance to one cycle of a sine wave. In Appendix 1, we show that such a recorded acceleration is produced by a source function with the time-dependence of (1).

According to the scaling laws [Cole, 1948], $\underline{a}$ and $2\pi/w_1$ are proportional to $E^{1/3}$, and S is independent of E. If we consider seismic waves whose wavelengths are large compared to $\underline{a}$ and whose periods are large relative to $2\pi/W_1$ then the source is adequately represented as an impulse in space and time given by

$$I = 2\pi \int_{-\infty}^{\infty} dt \int_{0}^{\infty} P_{zz}(r,o,t)\, r\, dr \quad . \tag{2}$$

I scales as E and can be used directly in the distance-amplitude relations derived by Haskell [1957] for Rayleigh waves. I is similar to the "reduced displacement potential" used by Werth and Herbst [1963] to represent seismic source functions of underground nuclear explosions in that both quantities scale as energy and both are independent of location in space and time of the point of observation.

From (2) it is clear that I is related to E according to

$$I/E = B \tag{3}$$

where B is a constant. The objective of this section is to evaluate B for the two target materials, sand and bonded sand.

Unconsolidated Sand. In Appendix 1 we show that the seismic impulse, I, is given by

$$I = GT \tag{4}$$

where $T = 2\pi/w_1$ is the observed period or duration of the accelerations recorded at the target surface and G is defined in Appendix 1. G is estimated from the observed maximum acceleration and the apparent duration of the signal. Table 3 lists values of G and T for eight impacts in sand used to determine I_1, the effective impulse in sand. Values of I_1/E (or B_1) in Table 3 show variation of about a factor of 6. The average value is

$$I_1/E = 0.6 \times 10^{-5} \pm 0.4 \times 10^{-5} \tag{5}$$

The scaling laws assumed here predict that values of T, listed in Table 3, should vary as $E^{1/3}$ but, in fact, T shows no systematic variation with E. One possible explanation is that waves with frequencies higher than about 2 Khz cannot propagate far enough through the sand to be observable. If so, then the estimates of I_1/E are underestimates. Considerations based on conservation of momentum, to be discussed later, also suggest that (5) is an underestimate.

Bonded Sand. The signals recorded in bonded sand (Figure 3) are more difficult to interpret in terms of the source function given by (1) because the seismic wavelengths are comparable to the target dimensions; hence, the observed signal is a combination of direct and reflected arrivals. The effective seismic impulse, I_2, applied to a bonded sand target was deduced by estimating the total kinetic energy in the elastic waves of an impacted target and then using an expression derived by Wolf [1944] that relates power radiated in the seismic waves to a time-varying vertical force applied to the surface. From this analysis, we show in Appendix 2 that the effective impulse in bonded sand can be obtained as

$$I_2 = \frac{1}{2\pi} \frac{(\rho \alpha^3 E_e T^3)^{1/2}}{.384} \tag{6}$$

where $T = 2\pi/w_1$ is the period of the source function as before, ρ and α are the density and compressional velocity respectively, and E_e is the

estimated seismic energy in the target. We see that I_2 scales as E since T scales as $E^{1/3}$ and E_e scales as E.

To determine I_2, it is necessary to calculate E_e and T. E_e, the seismic energy imparted to the target, is given by

$$E_e = 1/2\, M\bar{v}^2 \tag{7}$$

where M is the target mass and $\bar{v}$ is the root-mean-square velocity of the target material. $\bar{v}$ was estimated from velocities measured by the four accelerometers on each target. Uncertainty enters the estimate of $\bar{v}$ primarily because the spatial variation of $\bar{v}$ throughout the target is not known. Because the accelerometer signals recorded on bonded sand have a sinusoidal appearance, the velocity was taken to be the maximum acceleration divided by $2\pi f$, where f is the predominent signal frequency. Typically, f was of the order of 6 to 7 Khz.

The estimation of T, the period of the source function, is less direct for the bonded sand cases than it is for the sand cases. The frequency content and appearance of the signals recorded in bonded sand are determined largely by the size and shape of the targets; hence, little information regarding the period of the source can be deduced from these signals. For this study, T was estimated from data presented by Karpov [1963] for impacts in wax targets. Karpov noted that when a wax target is impacted by a projectile with a mass of 0.485 gm and a velocity of 4 km/sec, the crater reaches a maximum depth of 4 cm and then undergoes an elastic recovery to a depth of 3 cm in a total time of about 1.5 ms. Accordingly, we assume that the source function for elastic waves had a duration or period of about 1.5 ms. Since the compressional velocity of the wax (1.85 km/sec) is close to that of the bonded sand material (2.1 km/sec), we assume that the source function would have had a period of 1.5 ms in the bonded sand also. The periods of source functions for impacts of projectiles of different kinetic energies were determined by scaling from 1.5 ms according to $E^{1/3}$.

Table 4 lists values of E_e, T, I_2, and I_2/E for impacts in bonded sand. Although the values of I_2/E show some scatter, there is no systematic variation in the ratio with projectile energy. Within the uncertainties of the measurements I_2/E appears to be constant which tends to confirm the use of energy scaling. The average value of I_2/E for the eleven events in Table 4

is

$$I_2/E = 7.6 \times 10^{-5} \pm 3.3 \times 10^{-5} \quad (8)$$

which is approximately 12 times the corresponding value for sand targets. This difference in the value of I/E is not surprising in view of the difference in the elastic properties of the two materials (Table 1).

The most serious source of uncertainty in the determination of (8) is the estimation of T, the duration of the pressure source. It will be seen in equation (11) that the number of detectable meteoroids is proportional to I_2/E and, thus, from (6), to $T^{3/2}$.

Impacts and Explosions. Values of E_e/E, listed in Table 4 suggest that about 0.006% of the kinetic energy of a projectile is converted to seismic energy in a bonded sand target. Pomeroy [1963] stated that the corresponding figures for nuclear explosions detonated at the surface and 300 m underground are about 0.0015% and 0.5%, respectively. Thus, on the basis of coupling, impacts appear to be far more like surface than underground explosions.

Crater studies of impacts and explosions also suggest that impacts are similar to surface or near-surface explosions. Moore [1966] noted that with respect to crater formation, impacts appear to be similar to explosions detonated at a scaled depth, λ, of 0.25 to 0.5 feet, where $\lambda = \text{depth}/W^{1/3}$, and W is the energy release in equivalent pounds of TNT. For example, the crater formed by an impact with kinetic energy equal to the explosive energy of 1 kt of TNT, is similar to that formed by a 1 kt explosion detonated at a depth between 31.5 and 63 feet.

Momentum Conservation. Haskell [1957] stated that at low velocities of impact I ranges from mv for perfectly inelastic collisions to 2mv for perfectly elastic collisions, where mv is the projectile momentum. For hypervelocity impacts in which target and projectile damage are important considerations, I can exceed 2mv because ejecta from the crater add to the momentum imparted to the target. Values of I/mv plotted in Tables 3 and 4 indicate that impacts in sand are more inelastic processes than impacts in bonded sand. Values of I/mv that are less than 1 in Table 3 probably indicate that I has been underestimated. Otherwise, conservation of momentum is violated for these cases, assuming that the target does not move.

NUMBER OF DETECTABLE METEOROID IMPACTS

To estimate the number of impacts that will be detected during the lifetime of the passive seismic experiment, we use the source functions deduced in the previous section in conjunction with meteoroid flux statistics in the vicinity of the earth-moon system by Hawkins [Cosby and Lyle, 1965] and seismic distance-amplitude relations by Haskell [1957].

In this study meteoroids having masses from 10^{-2} to 10^{7} gms are considered as sources of impacts. Meteoroids of mass less than .01 gms, while they are important because of their large numbers, are not considered here since they produce signals in the frequency range above that detectable by the passive seismic instruments (20 Hz). Meteoroid impact in this mass range will probably contribute significantly to the signals recorded by the geophones used in the "active" seismic experiment which can detect frequencies as high as 250 Hz. Meteoroids having masses greater than 10^{7} gms are unlikely to impact the moon during any given year. For masses less than about 300 gms the cumulative influx rate to the earth according to Hawkins is

$$\log_{10} n = -13.09 - 1.34 \log_{10} m \tag{9}$$

where n is the cumulative influx per m^2/sec of meteoroids of mass m (gms) or larger. For masses greater than about 300 gms the influx, according to Hawkins, is

$$\log_{10} n = -14.23 - \log_{10} m \tag{10}$$

Values of n so determined must be divided by 2 to account for lunar shielding. The velocities of meteoroids impacting the moon range between 2.4 km/sec (lunar escape-velocity) and 73 km/sec. The kinetic energies of impacting meteoroids were obtained by assuming a root-mean-square velocity of 30 km/sec for meteoroids near the earth-moon system [Cosby and Lyle, 1965]. The necessity of assuming a mean velocity introduces more uncertainty into the estimation of detectable impacts because, as will be seen, the number of detectable impacts is proportional to I which, in turn, scales as v^2.

It is clear that the experiments used to deduce the empirical seismic-source functions, (5) and (8), are strictly relevant only for the lowest part of the actual velocity range of the meteoroids (2.4 to 7.3 km/sec) and a very small part of the mass range (0.25 - 5.0 gms). Thus, the application of (5) and (8) to the determination of the effectiveness of impacting meteoroids as seismic sources involves considerable, though unavoidable, extrapolation. The extrapolation in mass is not a very serious source of uncertainty, however, because, as will be seen, most of the detectable meteoroids have masses greater than 0.1 and less than 10 gms. (Table 5, Figure 8).

The radius of detectability of a meteoroid of mass m (or kinetic energy $E = 1/2\ mv_m^2$, v_m = 30 km/sec) was obtained using equations presented by Haskell [1957]. Haskell pointed out that for nontectonic seismic sources, such as impacts, Rayleigh waves always have the largest amplitudes of all seismic waves because most of the energy in the elastic wave field leaves the source in the form of Rayleigh waves and also because Rayleigh waves diminish more slowly with distance than body waves. Thus, we confine our attention to amplitudes of Rayleigh waves from impact sources; this obviates the need to consider, in detail, the interior structure of the moon.

It is easily shown that equations (3.1), (3.2), and (3.3) of Haskell [1957] are equivalent to

$$\log A = -D + \log I - 2 \log r \tag{11}$$

for Rayleigh waves with amplitude A recorded a distance r from a source with impulse I. The value of D in (11) depends on the quality factor, Q, assumed for the elastic medium. D = -3.948, -4.958, and -5.286 for Q = 500, 70, and 10 respectively (r and A in cm, I in gm-cm/sec). According to Haskell, these quality factors correspond to basement, sediment, and soil, respectively. In Haskell's treatment as well as the present study, the elastic medium is assumed to be homogeneous and isotropic. Furthermore, the duration of the impact is assumed short compared to the predominant seismic signal frequency.

Haskell also concluded that the predominant frequency in a Rayleigh wave signal is given by

$$fm = \frac{Qc}{2\pi r} \tag{12}$$

for Rayleigh waves with phase velocity c.

The maximum source (impact) - receiver (seismometer) separations for detection and corresponding predominant frequencies were computed for meteoroids of various masses using impulses appropriate for unconsolidated and bonded sand and three values of Q: six combinations of assumptions in all. The results are listed in Table 5 for the six assumptions. The number of meteoroid impacts per m^2/yr, n, is also listed as well as E, the kinetic energies of the meteoroids, and I_1 and I_2, the impulsive source functions from (5) and (8). A in (11) was determined from the response curves shown in Figure 7. Note that 0 db corresponds to a detectable signal amplitude of 10^{-7}cm. Predominant frequencies in Table 5 were computed by assuming that C = 2 km/sec for m = 0.01 and 0.1 gm, C = 2.5 km/sec for m = 1 and 10 gm, C = 3 km/sec for m = 100 gm, and C = 3.5 km/sec for $m \geq 1000$ gm.

The total number of detectable impacts was computed by integrating n(r) (interpolated between values given in Table 5) over the lunar surface and is given by

$$N = \iint n(r)\, dS$$

Figure 8 shows the number of meteoroid impacts that will be detected in various distance ranges for the six assumptions of coupling and dissipative properties of the target medium. For the least favorable set of assumptions, fewer than three meteoroid impacts will be detected during the experiment and for the most favorable conditions, about one impact per day will be recorded. The frequencies shown in Figure 8 are appropriate for the more distant end of each distance range. It can be seen that most of the detectable impacts will occur within 100 km of the recording site and will be recorded best by the short-period seismograph.

Results of a number of investigations indicate that much of the surface of the moon is covered with a fragmental layer of thickness ranging from about 1 to 10 m [e.g., Quaide and Oberbeck, 1968]. For any of the cases listed in Table 5, most detectable impacts which occur within 10 km of the seismometer will be due to meteoroids having masses of less than 10 gms or energies of less than 4.5×10^{13} ergs (equivalent to about 2 lbs of TNT). Such meteoroids cannot be expected to penetrate the fragmental surface layer and so the low-Q, low-coupling cases probably apply for these nearby events. At distances greater than 1000 km, on the other hand, all of the

detectable impacts will be caused by meteoroids with masses larger than 10^4 gms or energies greater than 4.5×10^{16} ergs (equivalent to about 2000 lbs of TNT). Such impacts would probably penetrate the fragmental layer to the hard rock beneath. Furthermore, a high value of Q is probably appropriate for the predominantly low-frequency waves from teleseismic events.

In addition to the uncertainties discussed above in connection with the derivation of equations (5) and (8), the seismic source relations for impacts, certain other potential error sources should be noted.

There is disagreement over meteoroid flux statistics in the vicinity of the earth-moon system. For example, meteoroid impact statistics deduced by Shoemaker [1966] would alter the predictions of Figure 8 in that more impacts due to large meteoroids (greater than 1000 gms) and fewer impacts due to small meteoroids would be detected.

Another uncertainty in the source function is the effect of nonvertical impact. Unfortunately, all of the impacts used in this study were at 0° angle of incidence. There is no obvious reason to expect that an oblique impact would be any more or less efficient for producing seismic waves than one at normal incidence, so that this should not be a serious source of error. One effect of oblique incidence would be an asymmetrical seismic radiation pattern at the source.

Another possible source of error is the likelihood of secondary impact events. Gault et al. [1964] have pointed out that the flux of fragments of a given mass that are ejected from the lunar surface is probably between three and four orders of magnitude greater than the flux of the impacting bodies of the same mass that produce the ejecta. Most of these fragments will be ejected from the lunar surface with less than escape velocity and so will cause secondary impact events. Thus, the predictions of Figure 8 may be shifted upward significantly by the addition of many impact events caused by fragments traveling at speeds ranging between near zero and 2.4 km/sec.

Finally, uncertainty in the structure of the elastic medium is a possible source of error in the predictions of Figure 8. The seismic distance-amplitude relations deduced by Haskell [1957], and used in this study, are based on the assumption of a homogeneous and isotropic elastic medium. Vertical stratification of the elastic medium has two effects on Rayleigh waves. It increases the amplitude of ground motion at the surface by channeling more of the total Rayleigh wave energy into the near-surface

layers (assuming an increase in shear velocity with depth). On the other hand, stratification introduces dispersion into the Rayleigh wave signal which causes the amplitude to be diminished.

Artificial Impact Sources. The above analysis can be used to determine the effectiveness of missile impacts as seismic sources. As an example we consider the impact of the spent Saturn S-IVB stage of the Apollo booster which has a mass of 1.6×10^6 gm. If used as a seismic source, it would have an impact velocity of about 2.6 km/sec or a kinetic energy of $5.41(10)^{16}$ ergs. For coupling similar to sand, use of (5) gives $I_1 = 3.24 \times 10^{11}$ gm-cm/sec. For coupling similar to bonded sand use of (8) gives $I_2 = 4.11 \times 10^{12}$ gm-cm/sec. The radius of detectability of the S-IVB can be computed by inserting the above values of I into equation (11). Table 6 lists the radii of detectability for six combinations of coupling and attenuation. The minimum detectable ground motion is assumed to have an amplitude of 10^{-7} cm. We see from Table 6 that the S-IVB could be of considerable use as a seismic source, especially if the coupling determined for bonded sand is appropriate for the moon.

Conclusions. Even with the considerable uncertainty inherent in a study such as this, it seems safe to conclude that meteoroids will definitely be a source of detectable seismic activity on the moon. The Apollo seismic experiments may, in fact, be the best means for determining the numbers of meteoroids in near-lunar space.

This work is presently being extended to much larger masses by the recording of seismic waves from missile impacts at White Sands Missile Range. Results from the missile impacts should reduce some of the uncertainty relative to the validity of extrapolating our empirical formulas to different mass ranges.

ACKNOWLEDGMENTS

We gratefully acknowledge the assistance of Stamatios Thanos for designing and testing most of the instrumentation used in this study, and that of Verne Oberbeck and John Wedekind for assistance in conducting a major portion of the experimental work at Ames Research Center. We are also indebted to Jack Oliver, Lynn Sykes, and Lee Alsop for critically reviewing the manuscript. We are grateful to Henry Moore of the U.S. Geological Survey for advice and assistance, particularly in the follow-on work now in progress.

The research was supported by the National Aeronautics and Space Administration (contract NAS 9-5957) and by a research grant from the Bendix Corporation.

Table 1. Bulk Properties of Targets

	α (km/sec)	β (km/sec)	ρ (gm/cm^3)
Unconsolidated Sand	0.13	0	1.63
Bonded Sand	2.12	1.24	1.63

Table 2. Summary of Impact Data

Shot No.	Maximum Accelerations (g's) Phone 1	Phone 2	Projectile Mass gms	Projectile Velocity km/sec	Projectile Momentum cgs	Projectile Kinetic Energy cgs	Target Material
30	0.60	1.10	0.290	6.93	$2.01\,(10)^{5}$	$6.97\,(10)^{10}$	sand
31	0.45	0.88	0.283	4.74	1.34	3.18	sand
32	0.70	1.90	0.286	6.01	1.72	5.16	sand
33	110	236	0.282	4.88	1.37	3.35	bonded sand
34	361	462	0.289	7.27	2.10	7.62	bonded sand
35	230	350	0.280	6.48	1.82	5.90	bonded sand
36	0.40	0.88	0.272	2.48	0.68	0.84	sand
37	0.35	0.55	0.273	1.62	0.44	0.36	sand
39	101	128	0.276	2.28	0.63	0.82	bonded sand
40	29	68	0.268	1.60	0.43	0.34	bonded sand
41	180	195	0.556	2.34	1.30	1.53	bonded sand
46	0.64	1.10	0.548	2.06	1.13	1.16	sand
52	250	200	4.704	1.79	8.44	7.58	bonded sand
53	0.88	1.20	0.441	4.83	2.13	5.16	sand
54	275	292	0.440	4.37	1.92	4.18	bonded sand
58	225	340	3.104	1.86	5.78	5.38	bonded sand
59	162	262	0.440	5.52	2.43	6.70	bonded sand
60	305	328	0.442	6.11	2.70	8.12	bonded sand
61	1.20	2.13	0.460	5.94	2.73	8.12	sand

Table 3: Factors Used in Calculation of Seismic Impulse in Sand
(Symbols defined in text.)

Shot No.	Maximum Accelerations cm/sec^2	Signal Period, T sec	G	I_1	I_1/E	I_1/mv
30	1.1×10^3	1.2×10^{-3}	9.57×10^7	1.15×10^5	1.65×10^{-6}	0.57
31	0.88×10^3	0.9×10^{-3}	5.74×10^7	5.17×10^4	1.62×10^{-6}	0.39
32	1.9×10^3	1.4×10^{-3}	1.96×10^8	2.78×10^5	0.54×10^{-5}	1.62
36	0.88×10^3	1.1×10^{-3}	7.02×10^7	7.72×10^4	9.19×10^{-6}	1.13
37	0.55×10^3	1.3×10^{-3}	5.18×10^7	6.73×10^4	1.87×10^{-5}	1.53
46	1.1×10^3	1.0×10^{-3}	7.98×10^7	7.98×10^4	6.88×10^{-6}	0.71
53	1.2×10^3	1.2×10^{-3}	1.85×10^8	2.22×10^5	2.73×10^{-6}	0.59
61	2.1×10^3	1.2×10^{-3}	1.04×10^8	1.25×10^5	2.42×10^{-6}	0.81

Table 4. Factors Used in Calculation of Seismic Impulse in Bonded Sand. (Symbols defined in text.)

Shot No.	Ee (ergs)	T^3 (sec^3)	$I_2 \times 10^6$	$I_{2/E} \times 10^{-4}$	I_2/mv	$E_{e/E} \times 10^{-5}$
33	8.3×10^5	2.91×10^{-9}	1.67	0.50	12.2	2.5
34	6.2×10^6	6.63×10^{-9}	6.89	0.90	32.8	8.1
35	3.1×10^6	5.13×10^{-9}	4.29	0.73	23.6	5.2
39	1.1×10^6	0.71×10^{-9}	0.95	1.16	15.0	13.4
40	3.1×10^5	2.97×10^{-10}	0.33	0.96	7.6	9.1
41	1.5×10^6	1.33×10^{-9}	1.52	0.99	11.7	9.8
52	3.1×10^6	$6.59. \times 10^{-9}$	4.86	0.64	5.8	4.1
54	2.5×10^6	3.64×10^{-9}	3.24	0.78	16.9	6.0
58	2.2×10^6	4.68×10^{-9}	3.24	0.60	5.6	4.1
59	1.5×10^6	5.83×10^{-9}	3.18	0.47	13.1	2.2
60	3.0×10^6	7.07×10^{-9}	4.95	0.61	18.1	3.7

Table 5. Maximum Range of Detection of Meteoroids and Predominant Signal Frequency as a Function of Meteoroid Mass.

Meteoroid Mass	Meteoroid Kinetic Energy E(ergs)	Meteoroid Flux n	UNCONSOLIDATED SAND						BONDED SAND					
			Seismic Impulse I_1(cgs)	Maximum range for detection (r) and predominant signal frequency (f)					Seismic Impulse I_2(cgs)	Maximum range for detection (r) and predominant signal frequency (f)				
				Q = 10		Q = 70		Q = 500		Q = 10		Q = 70		Q = 500	
				r	f	r	f	r	f	r	f	r	f	r	f
0.01 gm	4.5×10^{10}	0.54×10^{-3}	2.7×10^{5}	37.3m	85.4hz	54.5m	409hz	175m	910hz	3.4×10^{6}	133m	23.9hz	194m	115hz	620m	257hz
0.1	$\times 10^{11}$	0.26×10^{-4}	$\times 10^{6}$	118m	27.0	172m	129	553m	288	$\times 10^{7}$	402m	7.6	613m	36.4	1.96km	81.0
1.0	$\times 10^{12}$	0.13×10^{-5}	$\times 10^{7}$	373m	10.7	545m	51.0	1.75km	114	$\times 10^{8}$	1.33km	3.0	1.94km	14.4	6.20km	32.1
10.0	$\times 10^{13}$	0.63×10^{-7}	$\times 10^{8}$	1.18km	3.4	1.72km	16.2	5.53km	36.0	$\times 10^{9}$	4.20km	0.95	6.13km	4.54	19.6km	10.2
10^2	$\times 10^{14}$	0.31×10^{-8}	$\times 10^{9}$	3.73km	1.28	5.45km	6.1	17.5km	13.6	$\times 10^{10}$	13.3km	0.36	19.4km	1.72	62.0km	3.8
10^3	$\times 10^{15}$	0.93×10^{-10}	$\times 10^{10}$	11.8km	0.47	17.2km	2.3	55.3km	5.0	$\times 10^{11}$	42.0km	0.13	61.3km	0.64	196km	1.42
10^4	$\times 10^{16}$	0.93×10^{-11}	$\times 10^{11}$	37.3km	0.15	54.5km	0.72	175km	1.6	$\times 10^{12}$	109km	0.05	194km	0.20	620km	0.45
10^5	$\times 10^{17}$	0.93×10^{-12}	$\times 10^{12}$	100km	0.06	172km	0.23	553km	0.50	$\times 10^{13}$	188km	0.03	613km	0.06	1960km	0.14
10^6	$\times 10^{18}$	0.93×10^{-13}	$\times 10^{13}$	175km	0.03	545km	0.07	1750km	0.16	$\times 10^{14}$	332km	0.02	1120km	0.04	5460km	0.05
10^7	$\times 10^{19}$	0.93×10^{-14}	$\times 10^{14}$	305km	0.02	995km	0.04	5460km	0.05	$\times 10^{15}$	580km	0.01	1900km	0.02	5460km	0.05

Table 6. Radii of Detectability for an S-IVB Impact

	$I_1 = 0.6 \times 10^{-5} E$			$I_2 = 7.6 \times 10^{-5} E$		
Q	10	70	500	10	70	500
r (km)	41	60	191	146	213	681
f (hz)	0.14	0.65	1.46	0.04	0.18	0.41

REFERENCES

Brown, H., The density and mass distribution of meteoritic bodies in the neighborhood of the earth's orbit, First National Space Science Symposium, Nice, France, 1960.

Chabai, Albert J., On scaling dimensions of craters produced by buried explosives, J. Geophys. Res., 70, 5075-5098, 1965.

Cole, R.H., Underwater Explosions, Princeton University Press, Princeton, N.J., 1948.

Cosby, William A. and Robert G. Lyle, The Meteoroid Environment and Its Effects on Materials and Equipment, U.S. Government Printing Office: 779-741, 1965.

Gault, Donald E., William L. Quaide, and Verne R. Oberbeck, Impact cratering mechanics and structures, Presented at the Conference on Shock Metamorphism of Natural Materials at Goddard Space Flight Center, Greenbelt, Maryland, April 1966.

Gault, Donald E., Ezra D. Heitowit, and Henry J. Moore, Some observations of hypervelocity impacts with porous media, The Lunar Surface Layer-Materials and Characteristics, John W. Salisbury and Peter E. Glaser, Eds., Academic Press, New York and London, 1964.

Haskell, N.A., An estimate of the maximum range of detectability of seismic signals, AFCRC-TN-57-202, 1957.

Karpov, B.G., Transient response of wax targets to pellet impact at 4 km/sec, Report No. 1226, Ballistic Research Laboratories, Aberdeen Proving Ground, Maryland, 1963.

Kinslow, Ray, Collisions at high velocity, International Science and Technology, 38-47, April 1965.

Laster, Stanley J. and Frank Press, A new estimate of lunar seismicity due to meteorite impact, Phys. Earth Planet. Interiors, 1, 151-154, 1968.

Phinney, R.A. and D. L. Anderson, Internal temperatures of the moon, In: Report of the Tycho Study Group, University of Minnesota, 1965.

Pomeroy, Paul W., Long period seismic waves from large, near-surface nuclear explosions, Bull. Seismol. Soc. Am., 53, 109-149, 1963.

Press, F., P. Buwalda, and M. Neugebauer, A lunar seismic experiment, J. Geophys. Res., 65, 3097-3105, 1960.

Quaide, William L. and Verne R. Oberbeck, Thickness determinations of the lunar surface layer from lunar impact craters, J. Geophys. Res., 73, 5247-5270, 1968.

Shoemaker, E., New statistics for meteoritic materials in the neighborhood of the earth, Personal communication to F. Press, 1966.

Short, Nicholas M., Shock processes in geology, Journal of Geological Education, 14, 149-166, 1966.

Watson, G.N., A Treatise on the Theory of Bessel Functions, Cambridge University Press, 1962.

Werth, Glenn C. and Roland F. Herbst, Comparison of amplitudes of seismic waves from nuclear explosions in four mediums, J. Geophys. Res., 68, 1463-1475, 1963.

Wolf, Alfred, The equation of motion of a geophone on the surface of an elastic earth, Geophysics, 9, 29-35, 1944.

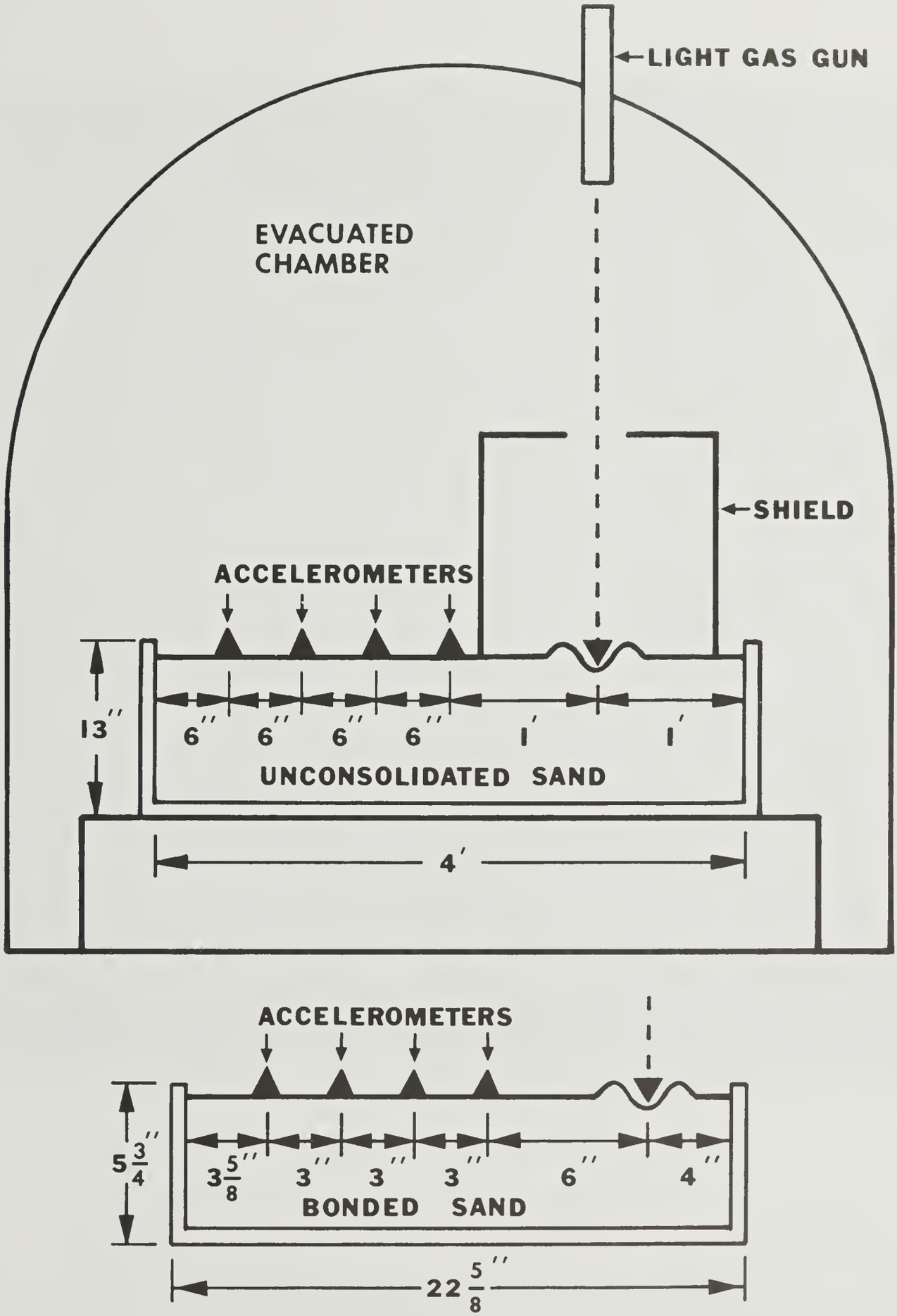

Figure 1: Schematic diagram of experimental apparatus used for impact experiments.

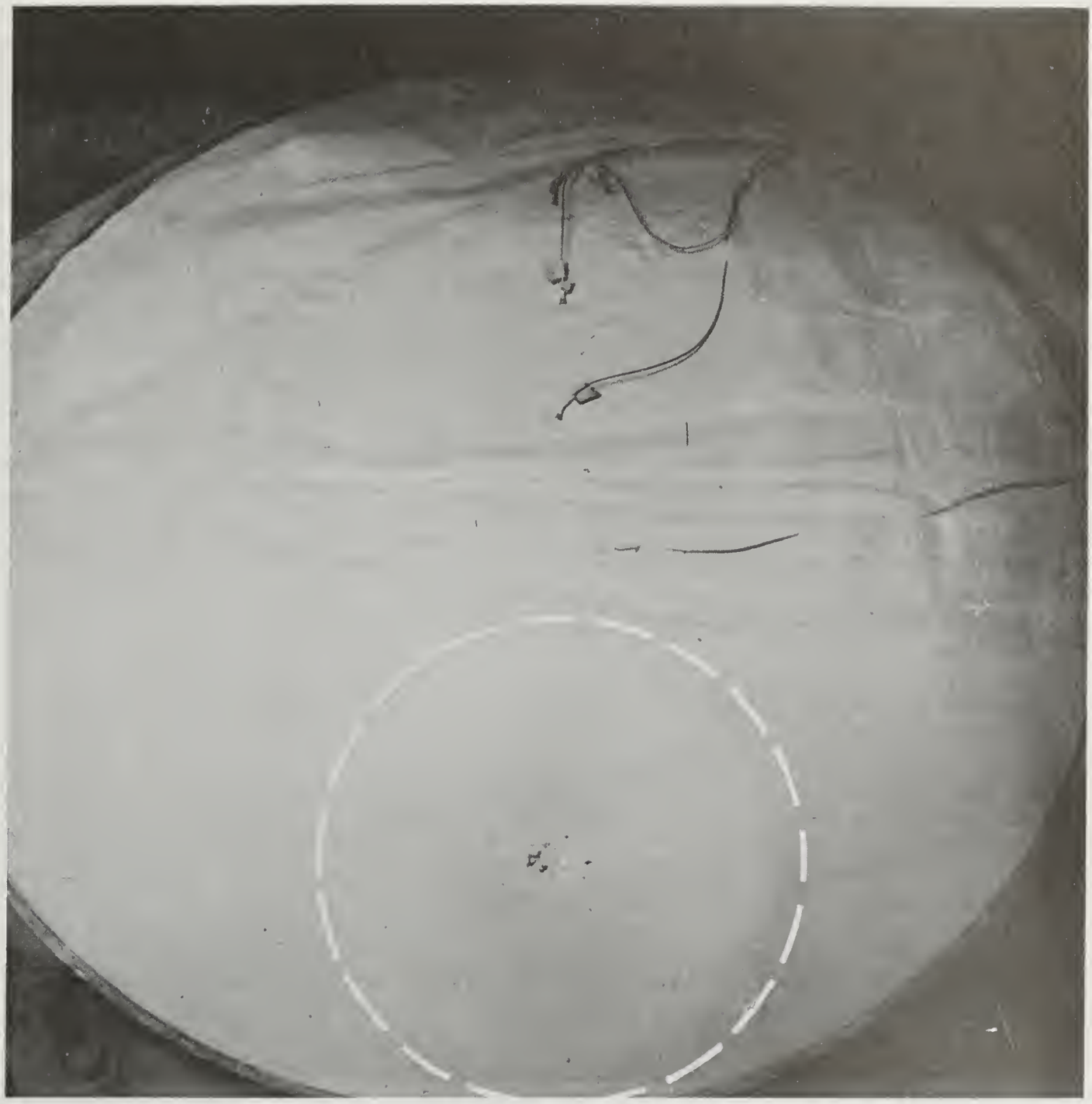

Figure 2a: Sand target after impact. Dashed white line outlines the impact crater. (Photograph courtesy of the National Aeronautics and Space Administration, Ames Research Center, Moffett Field, California)

Figure 2b: Bonded sand target after impact. (Photograph courtesy of the National Aeronautics and Space Administration, Ames Research Center, Moffett Field, California)

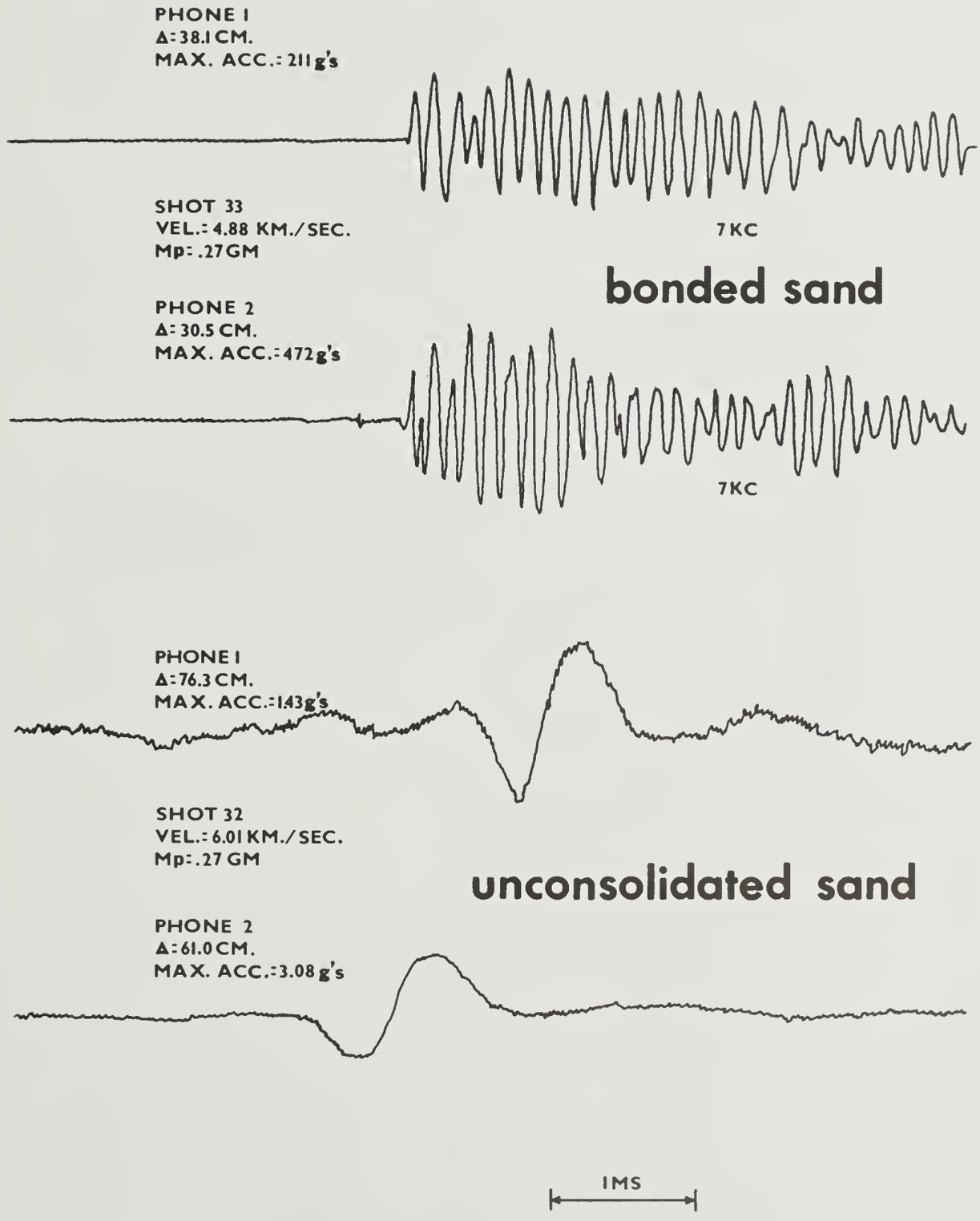

Figure 3: Typical seismic signals recorded in both types of targets. The signals shown were recorded by the most distant and second most distant accelerometers from the point of impact.

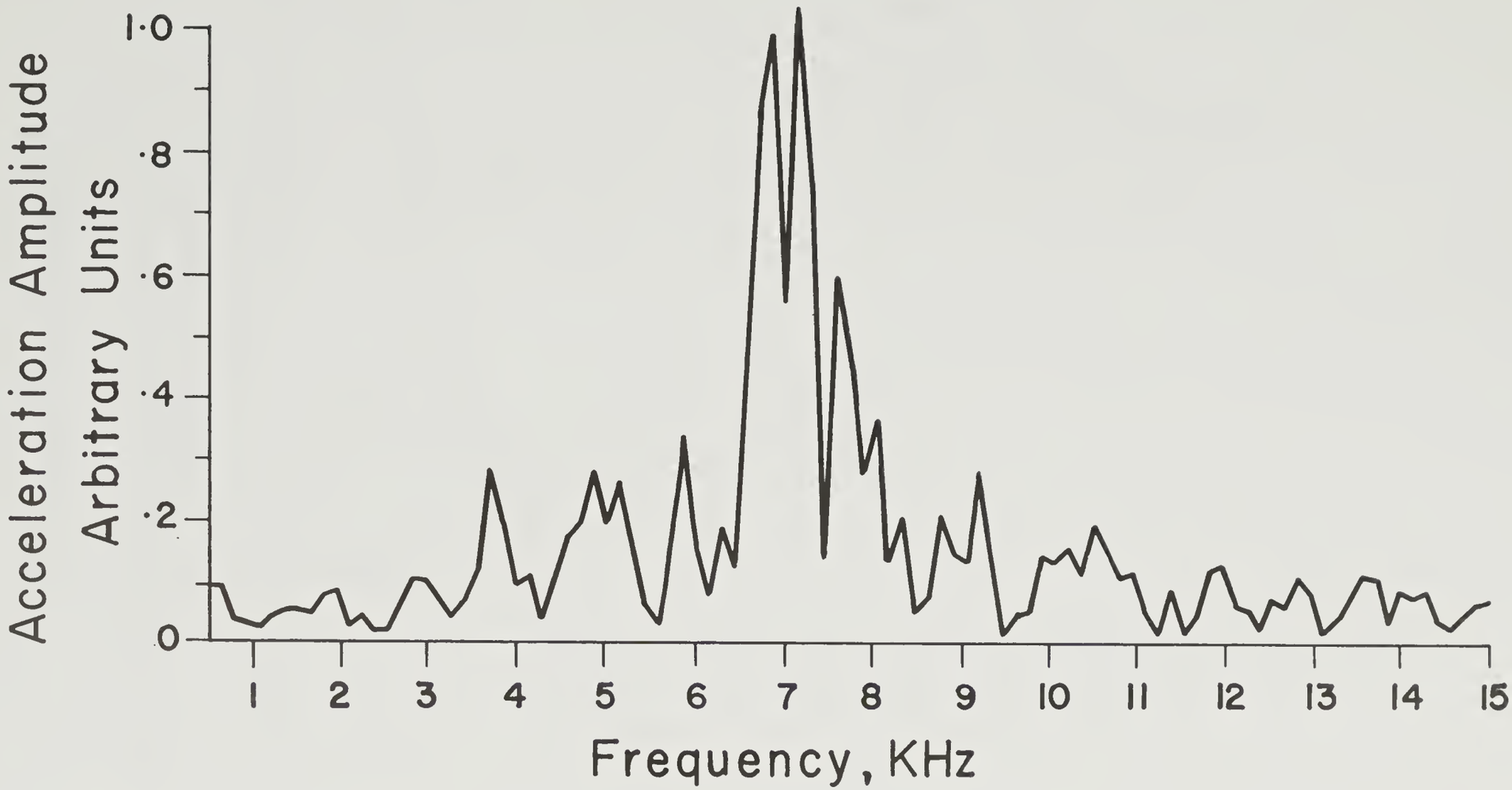

Figure 4: Spectrum of acceleration amplitude recorded by an accelerometer 31.0 cm from the point of impact in bonded sand.

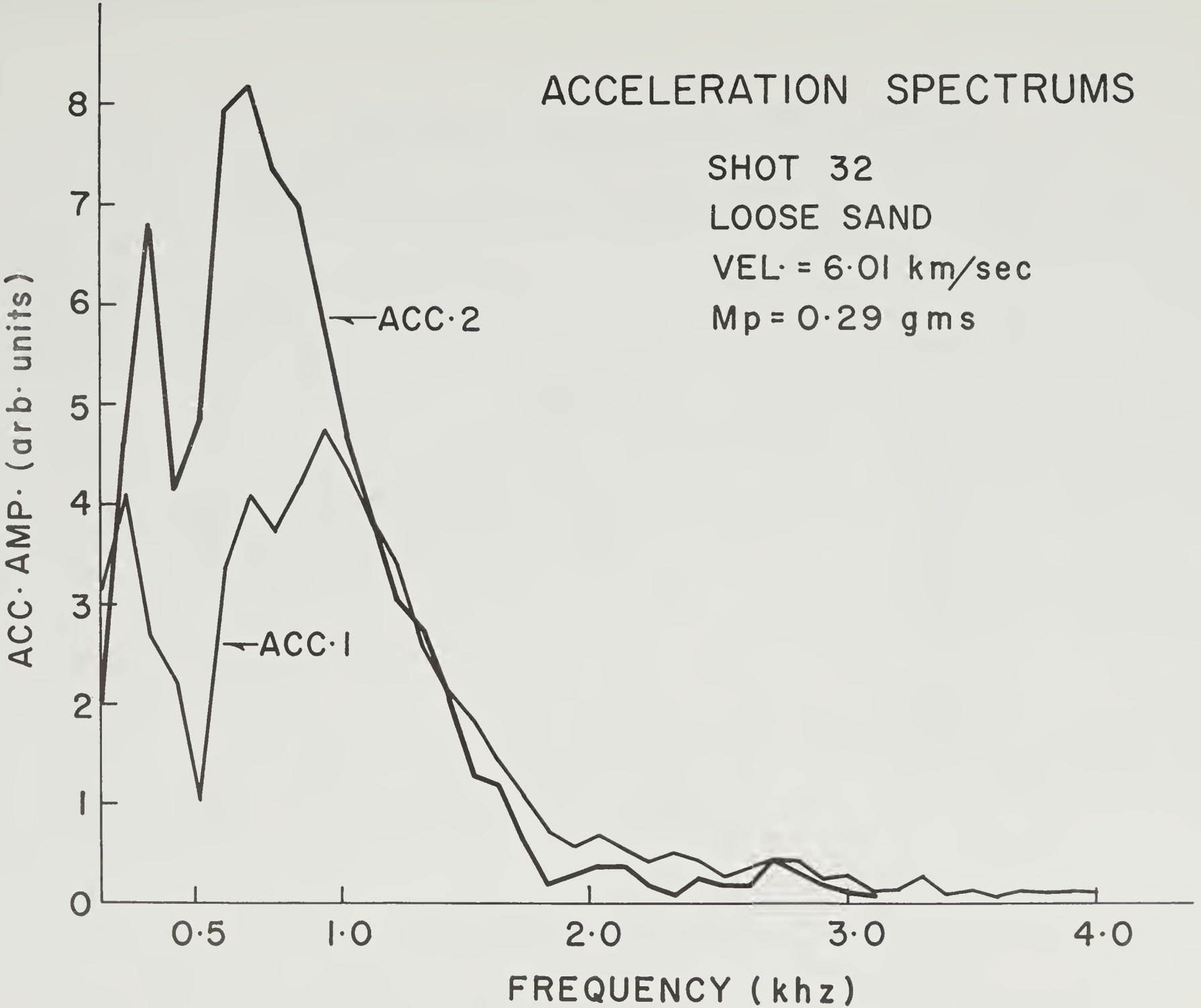

Figure 5: Spectrums of acceleration amplitude recorded by accelerometers 76.3 cm and 61.0 cm from the point of an impact in loose sand.

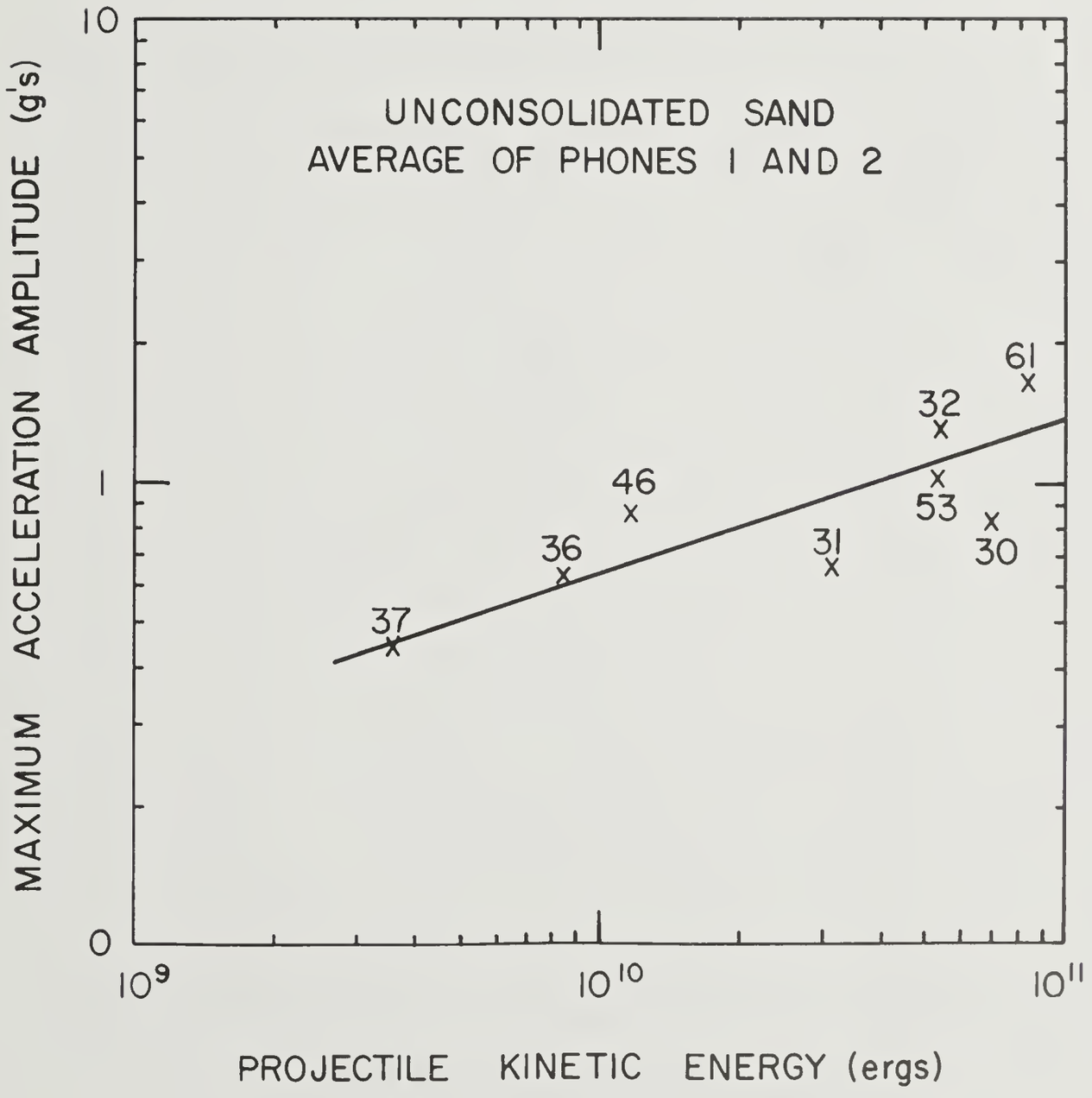

Figure 6a: Maximum acceleration recorded in a sand target as a function of projectile kinetic energy. The slope of the line is about 1/3.

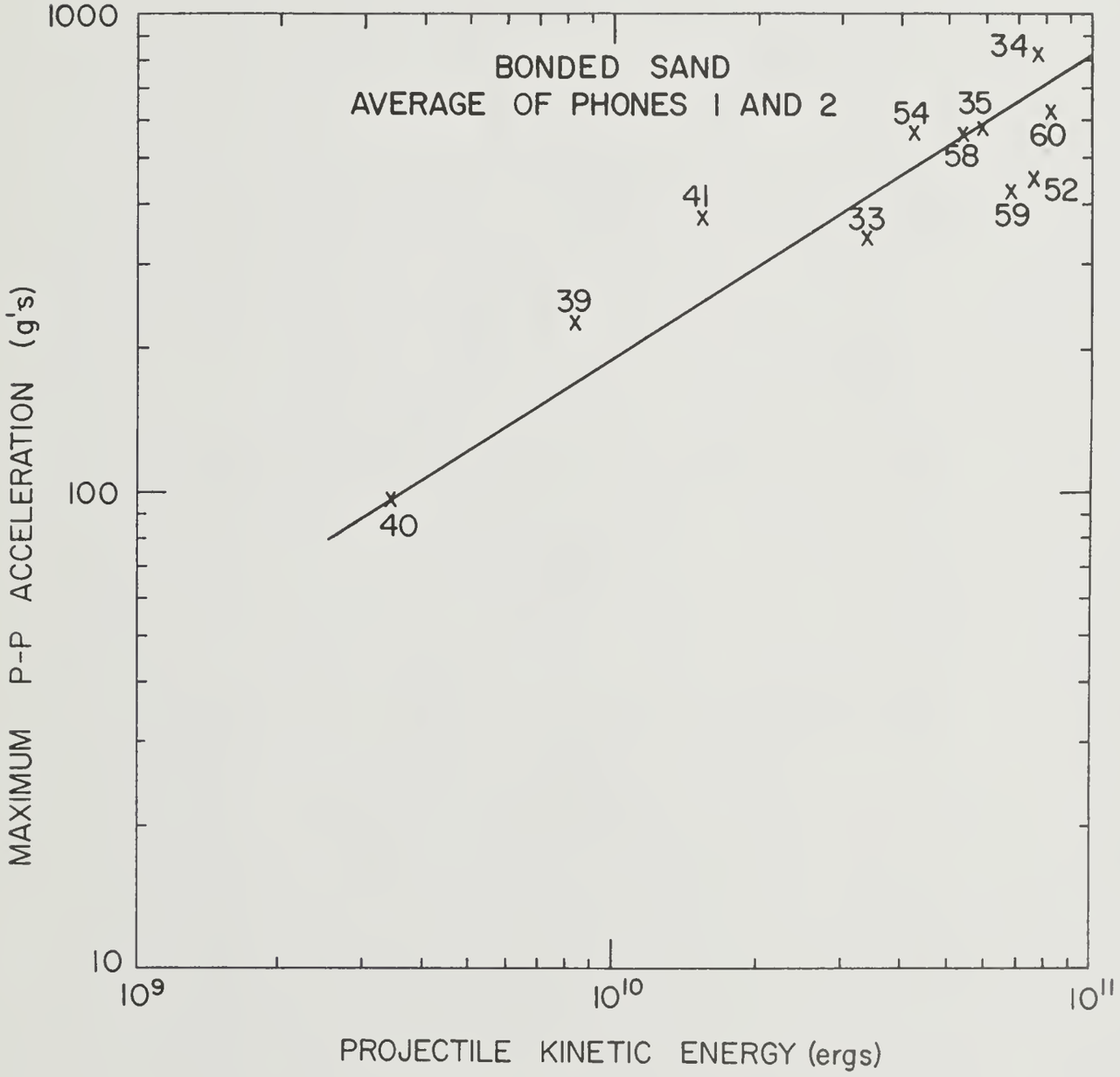

Figure 6b: Maximum acceleration recorded in a bonded-sand target as a function of projectile kinetic energy. The slope of the line is about 2/3.

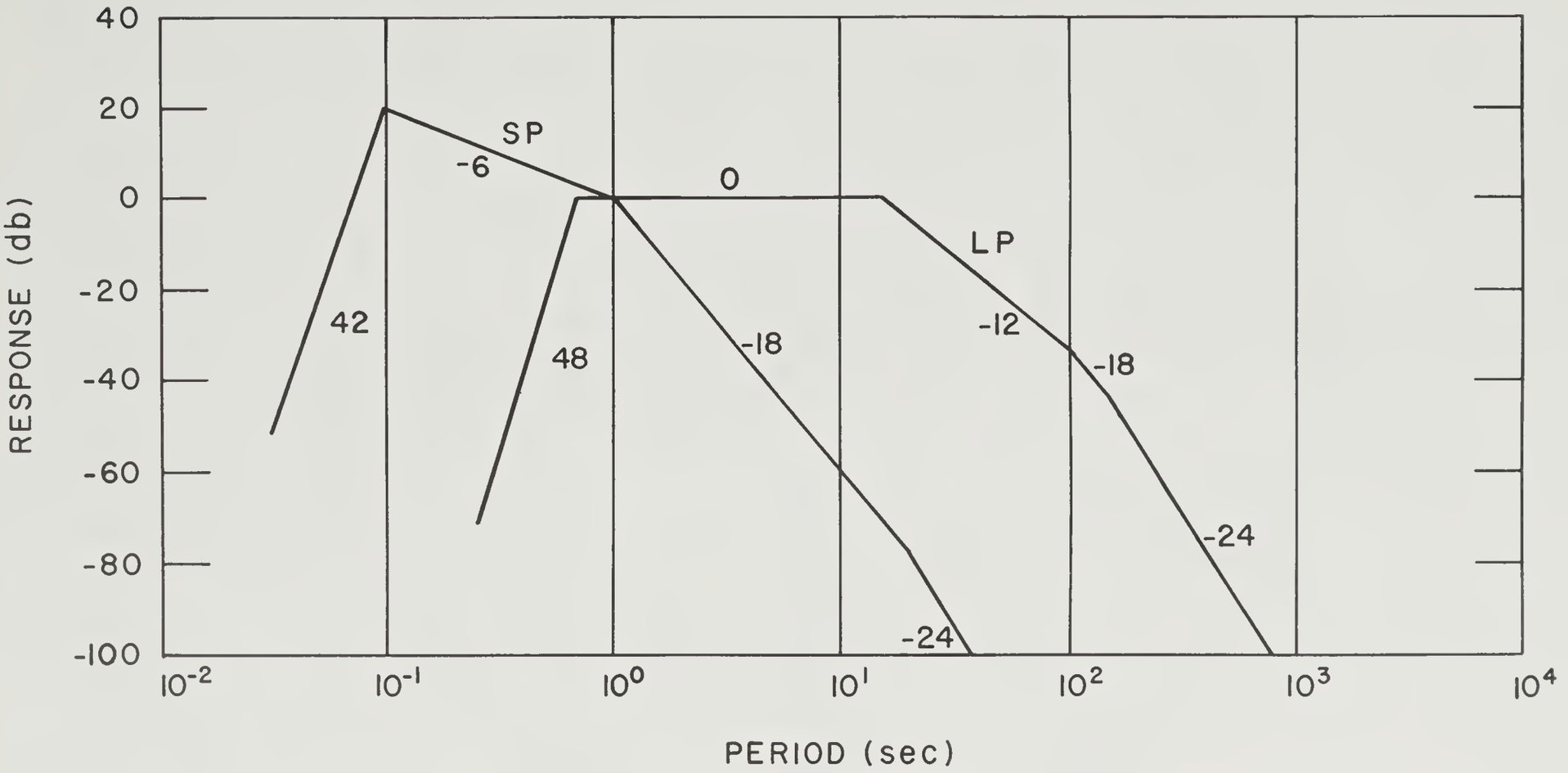

Figure 7: Nominal response curves for seismometers used in the passive seismic experiment.

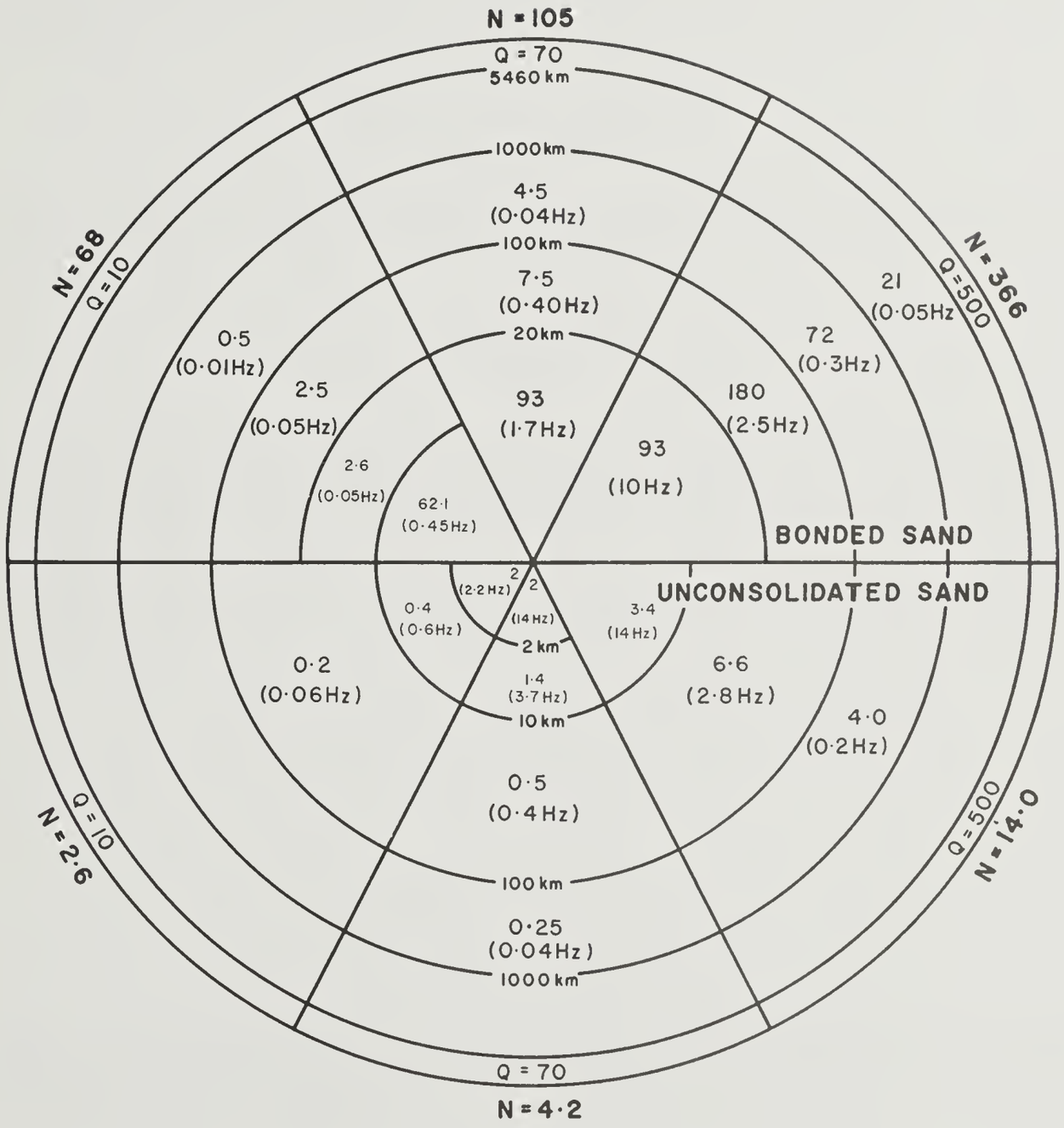

Figure 8: Number of meteoroid impacts detected in various distance ranges for the six assumptions discussed in the text. The predominant signal frequencies which appear in parentheses are appropriate for the most distant end of a particular distance range.

APPENDIX I

To determine B in (3) for the loose sand targets, let f(t) be the force applied to the surface of the target at the point of impact and its Fourier transform

$$F(w) = \int_{-\infty}^{\infty} e^{-iwt} f(t)\, dt \tag{A1}$$

Then the Fourier transform of the vertical stress representing the impact source is

$$P(r, o, w) = \frac{F(w)}{2\pi} \int_{o}^{\infty} Jo(kr)k\, dk \tag{A2}$$

to the extent that the spatial dependence of the source can be expressed as a Dirac delta function; i.e., assuming seismic wavelengths that are large compared to the source dimension.

If ϕ is the displacement potential of the Fourier transform of the seismic wave then

$$\phi = \frac{1}{2\pi} A(k, w) e^{-\nu z} Jo(kr)dk \tag{A3}$$

where

$$\nu = \sqrt{k^2 - k_\alpha^2}, \qquad k_\alpha = \frac{w}{\alpha}$$

In this analysis the sand targets are assumed to be equivalent to a bucket of liquid since the shear velocity is negligibly small compared to the compressional velocity, (Table 1).

The Fourier transform of the vertical displacement, d, is

$$\bar{d} = \frac{\partial \phi}{\partial z} \tag{A4}$$

At z = o

$$P(r,o,w) = -\rho w^2 \phi \tag{A5}$$

and so

$$A(k,w) = \frac{-kF(w)}{2\pi\rho w^2} \tag{A6}$$

and thus

$$\bar{d}(r,o,w) = \frac{F(w)}{2\pi\rho w^2} \int_0^\infty kJo(kr)dk \tag{A7}$$

According to Watson [1962, p 434]

$$\int_0^\infty \sqrt{k^2 - k_\alpha^2}\; kJo(kr)dk = \frac{r^{-3/2}(ik_\alpha)^{3/2} 2^{3/2}}{\Gamma(-1/2)} K_{3/2}(rk_\alpha i) \tag{A8}$$

For large values of its argument

$$K_{3/2}(rk_\alpha i) = \sqrt{\frac{\pi}{2rk_\alpha i}}\, e^{-irk_\alpha} \tag{A9}$$

and so for large values of rk_α

$$w^{-2}\, d(r,o,w) = \frac{w F(w) i e^{-ik\, r}}{\pi\rho\alpha\, r^2}$$

After transformation back into the time domain we obtain for the vertical acceleration at the surface of the sand target

$$\ddot{d}(r,o,t) = \frac{-ie^{-\delta r}}{2\pi^2\rho\alpha\, r^2} \int_{-\infty}^{\infty} w\, F(w)\, e^{iw(t-r/\alpha)} dw \tag{A10}$$

$$= \frac{ie^{-\gamma r}}{\pi \rho \alpha r^2} f'(t-r/\alpha)$$

where the factor $e^{-\gamma r}$ has been included to account for dissipation due to inelastic effects. Measurement of the decrease in signal amplitude with increasing distance from the impact yielded an average value of γ of 0.01/cm for the sand targets.

If the time dependence of the source function is

$$f(t) = G(1 - \cos w_1 t), \quad o \leq t \leq \frac{2\pi}{w_1} \tag{A11}$$

$$= 0 \quad , \text{otherwise}$$

then $f'(t) = Gw_1 \sin w_1 t$ for $o \leq t \leq \frac{2\pi}{w_1}$, which agrees qualitatively with the observed seismic signals in sand (Figure 3).

The seismic impulse is given by

$$I = \int_{-\infty}^{\infty} f(t)\, dt = GT \tag{A12}$$

where $T = \frac{2\pi}{w_1}$, the observed period or duration of the acceleration of a signal in sand. G is estimated by inserting (A11) into (A10) to obtain

$$G = \frac{AmTe^{\gamma r} \rho \alpha r^2}{2} \tag{A13}$$

where Am is the maximum acceleration of the signal as defined previously (Table 2).

APPENDIX II

According to Wolf [1944], the average power radiated into an elastic medium by a force with amplitude R and time dependence e^{iwt} is given by

$$P = \frac{.384\, w^2 R^2}{\rho \alpha^3} \tag{A14}$$

where ρ and α are the density and compressional velocity, respectively. The numerical coefficient holds for Poisson's ratio equal 0.25. The source function, suggested by signals recorded in sand, is taken to be the vertical force on the free surface of the target

$$\begin{aligned} H(t) &= R(1 - \cos w_1 t) \quad \text{for} \quad o \leq t \leq \frac{2}{w_1} \\ &= 0 \qquad\qquad \text{otherwise} \end{aligned} \tag{A15}$$

Although (A14) is appropriate for a steady state force, it can be used to determine that the energy radiated into the target by the force, (A15), is given to an adequate approximation by

$$E_e = \frac{2\pi}{w_1} P = \frac{2\pi(.384) w_1 R^2}{\rho \alpha^3} \tag{A16}$$

From (2) the seismic impulse is given by

$$I_2 = \frac{2\pi R}{w_1} \tag{A17}$$

and so

$$I_2 = \frac{1}{2\pi} \frac{(\rho^2 \alpha^3 E_e T^3)^{1/2}}{.384} \tag{A18}$$

where $T = \frac{2\pi}{w_1}$.

COLUMBIA LIBRARIES OFFSITE
CU90641795